MOLECULAR IMAGING AND BIOLOGY

Mol Imaging Biol (2019) 21:1127–1137
DOI: 10.1007/s11307-019-01346-1

Published Online: 7 March 2019

WMIS World Molecular Imaging Society

Check for updates

RESEARCH ARTICLE

Validation of *R*-2-[^{18}F]Fluoropropionic Acid as a Potential Tracer for PET Imaging of Liver Cancer

Zhanwen Zhang,[1,2] Shaoyu Liu,[1] Hui Ma,[1] Dahong Nie,[1] Fuhua Wen,[1] Jing Zhao,[1] Aixia Sun,[1] Gongjun Yuan,[1] Shu Su,[1] Xianhong Xiang,[1] Ping Hu,[2] Ganghua Tang[1]

[1]*Department of Nuclear Medicine and Medical Imaging, Guangdong Engineering Research Center for Translational Application of Medical Radiopharmaceuticals, The First Affiliated Hospital, Sun Yat-sen University, Guangzhou, 510080, China*
[2]*Department of Nuclear Medicine, The Sixth Affiliated Hospital, Sun Yat-sen University, Guangzhou, 510655, China*

Abstract

Purpose: 2-[^{18}F]Fluoropropionic acid (RS-[^{18}F]FPA) has shown potential value as a short-chain fatty acid positron emission tomography (PET) tracer for the detection of liver cancer. However, RS-[^{18}F]FPA is a mixture of 2-*R*-[^{18}F]fluoropropionic acid (R-[^{18}F]FPA) and 2-*S*-[^{18}F]fluoropropionic acid (S-[^{18}F]FPA). The aim of this study is to validate the feasibility of R-[^{18}F]FPA in preclinical PET imaging of liver cancer and to compare the use of R-[^{18}F]FPA with that of RS-[^{18}F]FPA and S-[^{18}F]FPA.

Procedures: A comparative study of R-[^{18}F]FPA, RS-[^{18}F]FPA, S-[^{18}F]FPA, and [^{18}F]FDG micro-PET imaging was performed in HepG2 and SK-Hep-1 tumor-bearing mice. A comparison of R-[^{18}F]FPA uptake with that of S-[^{18}F]FPA by HepG2 and SK-Hep-1 cells was made at different time points. Additionally, *in vivo* blocking experiments in HepG2 and SK-Hep-1 tumor models were conducted with orlistat and 3-nitropropionic acid (3-NP). *In vitro* blocking experiments with orlistat or 3-NP were performed with HepG2 and SK-Hep-1 cells.

Results: The radioactivity uptake values of R-[^{18}F]FPA were comparable to those of RS-[^{18}F]FPA but were higher than those of S-[^{18}F]FPA and 2-deoxy-2-[^{18}F]fluoro-D-glucose ([^{18}F]FDG) in HepG2 tumors. The radioactivity uptake values of R-[^{18}F]FPA in large HepG2 tumors were lower than those of [^{18}F]FDG ($P < 0.05$), while R-[^{18}F]FPA PET was significantly superior to [^{18}F]FDG PET in detecting small tumors (both SK-Hep-1 and HepG2 tumors). The *in vivo* PET imaging experiments showed that R-[^{18}F]FPA uptake in HepG2 tumor-bearing mice was blocked by 19.3 % and 31.8 % after treatment with orlistat and 3-NP, respectively. The radioactivity uptake values of R-[^{18}F]FPA in SK-Hep-1 tumor-bearing mice was blocked by 39.5 % with orlistat.

Conclusion: R-[^{18}F]FPA seems to be more potential than S-[^{18}F]FPA as an optically pure PET probe, with effective compensation for the deficiencies of [^{18}F]FDG, particularly in PET imaging of small liver cancer. The uptake mechanism of [^{18}F]FPA in liver cancer may be related to fatty acid synthesis and the tricarboxylic acid cycle. However, compared with the racemic RS-[^{18}F]FPA, the possible advantages of *R*-enantiomer R-[^{18}F]FPA still needs further research.

Zhanwen Zhang and Shaoyu Liu contributed equally to this work.
Electronic supplementary material The online version of this article (https://doi.org/10.1007/s11307-019-01346-1) contains supplementary material, which is available to authorized users.

Correspondence to: Ping Hu; *e-mail:* p.hu@zsyth.com, Ganghua Tang; *e-mail:* gtang0224@126.com

Key words: 2-[18F]Fluoropropionic acid, *R,S*-enantiomer, Liver cancer, Positron emission tomography, Uptake mechanism

Introduction

Primary liver cancer is the third leading causes of cancer-related deaths worldwide and is expected to become the third leading cause of cancer death in USA by 2030 [1]. The most common primary liver cancer in adult and children was hepatocellular carcinoma and hepatoblastoma, respectively [2, 3]. However, the sensitivities for detecting liver cancer using abdominal ultrasound (US), computed tomography (CT), and magnetic resonance imaging (MRI) are very low, particularly for lesions smaller than 2 cm [4, 5]. The detection of liver cancer at an early stage has become a great challenge for conventional imaging methods. Positron emission tomography (PET) using 2-deoxy-2-[18F]fluoro-D-glucose ([18F]FDG) is an excellent technique for diagnosing and staging various cancers. However, many studies have indicated that [18F]FDG PET imaging of liver cancer is relatively insensitive, particularly for well-differentiated hepatocellular carcinoma or small hepatocellular carcinoma lesions [6, 7]. Due to these limitations, there is a high demand for seeking other PET tracers to complement [18F]FDG PET imaging.

Lipid-related metabolic pathways are frequently upregulated in multiple types of cancer because abnormal fatty acid metabolism plays a crucial role in the proliferation and metastasis of tumor cells [8–11]. Several lipid-based PET radiotracers, such as [11C]acetate ([11C]AC), [18F]fluoroacetate ([18F]FAC), [11C]choline, and [18F]fluorocholine, have been developed to make up for the deficiencies of [18F]FDG in liver cancer and have a high sensitivity that is complementary to [18F]FDG PET imaging [12–23]. However, for some liver cancers with high radioactive accumulation of [18F]FDG, those lipid-related tracers was not obviously superior to [18F]FDG in PET/CT [15–17, 23]. In addition, the short half-life of ^{11}C ($t_{1/2}$ = 20.4 min) limits the widespread application of [11C]AC and [11C]choline [15, 16, 18, 19].

Fatty acid synthase (FASN) is a key enzyme in fatty acid synthesis that is overexpressed in multiple human cancers but exists at low levels in most normal human tissues [8–10]. Previous studies have demonstrated that the mechanism of [11C]acetate uptake in cancer involves FASN [10, 14, 22, 24]. Besides, FASN inhibition has been reported to be effective in reducing [11C]AC uptake in association with fatty acid synthesis [11, 24]. Propionic acid, like acetate, as a short-chain fatty acid, can be converted into succinyl coenzyme A through a multistep metabolic process *in vivo*, and then enters the tricarboxylic acid cycle pathway or acetyl coenzyme A pathway to participate in fatty acid synthesis [11, 14, 19, 21, 25–28]. Previous studies demonstrated that 2-[18F]fluoropropionic acid (RS-[18F]FPA), as an analog of [11C]AC, could be used for PET imaging of prostate cancer [25]. Thus, a hypothesis was suggested that RS-[18F]FPA, as an analog of [11C]AC, could be involved in fatty acid synthesis.

Our previous studies showed that R-[18F]FPA was superior to S-[18F]FPA and had similar potential to RS-[18F]FPA in PET imaging of prostate cancer [29], and RS-[18F]FPA could be used for PET imaging of liver cancer [30]. However, RS-[18F]FPA is a mixture of 2-*R*-[18F]fluoropropionic acid (R-[18F]FPA) and 2-*S*-[18F]fluoropropionic acid (S-[18F]FPA). The biological effectiveness of RS-[18F]FPA and its two chiral isomers may be different in PET imaging of liver cancer. As far as we know, biological evaluations of two chiral isomers of RS-[18F]FPA, R-[18F]FPA and S-[18F]FPA, for PET imaging of liver cancer has not been reported. In this work, it is necessary to compare the preclinical PET imaging feasibility of RS-[18F]FPA with that of its enantiomers R-[18F]FPA and S-[18F]FPA in liver cancer as compared with [18F]FDG. Additionally, it is not clear whether the uptake mechanism of [18F]FPA is related to FASN and the TCA cycle; therefore, the mechanism of [18F]FPA uptake in liver cancer was also explored in this study.

Materials and Methods

Chemicals and Equipment

All chemical reagents and solvents were purchased from commercial sources. Kryptofix 2.2.2 ($K_{2.2.2}$), acetonitrile (MeCN), *tert*-butyl alcohol (*t*-BuOH), (R)- and (S)-ethyl-2-(((trifluoromethyl)sulfonyl)oxy)propanoate), and methyl-2-bromopro-pionate were obtained from Sigma-Aldrich (Shanghai) Trading Co. Ltd. The Sep-Pak light QMA, Sep-Pak plus Alumina-N and Oasis HLB cartridges were obtained from Waters (Milford, USA), and Grace SCX cartridges were purchased from Alltech (Deerfield, USA). Radioactivity was measured by a gamma counter (γ-counter) (SN-6105, Shanghai Nuclear Rihuan Photoelectric Instrument LLC, China).

Radiosynthesis of R-[18F]FPA, S-[18F]FPA, and RS-[18F]FPA

R-[18F]FPA or S-[18F]FPA was synthesized from the chiral precursor (S)- or (R)-ethyl 2-(((trifluoromethyl)sulfonyl)oxy)propanoate), respectively, *via* a two-step reaction, consisting of [18F]fluorination and on-column hydrolysis reaction described in detail by our earlier paper [29, 31]. RS-[18F]FPA was synthesized from

the precursor ethyl-2-bromopropionate [31]. The radiosynthesis of RS-[18F]FPA, R-[18F]FPA, and S-[18F]FPA was performed in a commercial FDG synthesizer (Beijing Sunvic Medical Technology Co, Ltd) with a modification as described previously [29, 31]. The total decay-corrected radiochemical yields of RS-[18F]FPA, R-[18F]FPA, and S-[18F]FPA were over 40 %, with a specific activity of around 40 GBq/μmol. The radiochemical purities of RS-[18F]FPA, R-[18F]FPA, and S-[18F]FPA were over 95 %, and their enantiomeric purities were above 95 % [29].

In vitro Cell Uptake and Inhibition

Human hepatoblastoma cell line HepG2 and human hepatocellular carcinoma cell line SK-Hep-1 were obtained from the Cell Bank of the Chinese Academy of Sciences (Shanghai, China). The cells were cultured in DMEM containing 10 % fetal calf serum at 37 °C in a humidified atmosphere of 5 % CO_2. Twenty-four hours before the cell uptake experiments, the HepG2 or SK-Hep-1 cells ($1–2 \times 10^7$) were seeded in 24-well plates. The cells were grown to ~70–80 % confluence in growth medium for the uptake experiments. Approximately 0.185 MBq (5 μCi) of R-[18F]FPA or S-[18F]FPA in 1.0 ml of fresh media was added to each well. A total of 5, 30, 60, or 90 min later, the culture medium containing the radioactive substance was removed. To stop the uptake of tracers, ice-cold phosphate-buffered saline (PBS) was used to rinse away any residual radioactivity three times. The cells were lysed by using 500 μL of 0.5 N NaOH for 30 min at room temperature. Samples were counted with a γ-counter and then measured for protein content by using a standard copper acid assay (BCA, Pierce Biotechnology) using bovine serum albumin as the protein standard.

To compare the abilities of different concentrations of orlistat to inhibit fatty acid synthesis or of 3-nitropropionic acid (3-NP) to inhibit the TCA cycle [9, 24, 32], the original medium was replaced with fresh growth medium containing orlistat (0, 25, 50, 100, 200, or 400 μM) or 3-NP (0, 25, 50, 100, 200, or 400 μM). Orlistat and 3-NP were dissolved in dimethyl sulfoxide (DMSO) (< 1 %), and the control groups received DMSO (0.1 %) only. Then, 200 μL of RS-[18F]FPA, S-[18F]FPA, or R-[18F]FPA (5 μCi) was added to each well. After 30 min, the incubation was terminated, and then the radioactive liquid was removed. The methods of cell lysis and radioactivity counting were the same as those mentioned above. These experiments were repeated three times on different days.

Animal Models

Mice were purchased from the Laboratory Animal Center of Sun Yat-sen University (Guangzhou, China) and housed 5–6 animals per cage under standard laboratory conditions. Human hepatoblastoma HepG2 cells (1×10^7) and hepatocellular carcinoma SK-Hep-1 cells (1×10^7) were injected subcutaneously into BALB/c nude mice (4 weeks old, weighing 25–30 g, male). PET-CT imaging was performed when the tumors grew to approximately 5–10 mm in diameter. The experiments were approved by the Institutional Animal Care and Utilization Committee (IACUU) of the First Affiliated Hospital, Sun Yat-Sen University (approval no. 2016058).

Small-Animal PET Imaging

The nude mice with human liver cancer were fasted for at least 6 h before micro-PET scanning. The tumor-bearing mice were injected intravenously with 3.7–5.5 MBq (100–150 μCi in 0.1 ml of saline) of RS-[18F]FPA, S-[18F]FPA, R-[18F]FPA, or [18F]FDG sequentially over 4 days. The mice were anesthetized with 2 % pentobarbital (5 ml/kg) before the PET scanning and remained anesthetized during scanning [31]. Static small-animal PET-CT images (10-min low-dose CT scan and 10-min static PET scan) were acquired 30, 60, 90, and 120 min after injection. Image reconstruction and quantification were performed as described previously [29, 30].

Ex vivo Biodistribution of R-[18F]FPA

HepG2 tumor-bearing BALB/c nude mice were divided into four groups ($n = 3$ per group), and each mouse was injected through the tail vein with 0.74 MBq (20 μCi) of R-[18F]FPA in 0.2 ml of saline. Mice were euthanized by cervical dislocation 30, 60, 90, and 120 min after injection. Blood samples from the orbital sinus and the organs of interest (brain, heart, lungs, liver, kidneys, pancreas, spleen, stomach, intestines, muscle, bone, and tumor) were harvested, blotted dry, and weighed quickly, and [18F] radioactivity was measured with a γ-counter [29]. All measurements were background-subtracted and decay-corrected to the time of injection and then averaged together. The data are expressed as percentage injected dose per gram of tissue (% ID/g).

Small-Animal PET Assessment of FASN and TCA Inhibition

Twenty-four hours after PET imaging with R-[18F]FPA, the same mice ($n = 3$) received intraperitoneal injections of orlistat at 240 mg/kg or 3-NP at 35 mg/kg dissolved in DMSO (< 2 % DMSO). Sixty minutes after injection of the orlistat or 3-nitropropionic acid, the mice were again injected intravenously with 3.7–5.5 MBq (100–150 μCi, 0.1 ml of saline) of R-[18F]FPA, and the mice then underwent PET scanning again following the same protocol [9, 24, 32].

Statistical Analysis

All data are expressed as the mean ± standard deviation (SD). The statistical analysis was performed with SPSS software version 20.0 (SPSS Inc.) for Windows (Microsoft). Comparisons between conditions were performed by using unpaired, two-tailed Student's *t* tests. $P < 0.05$ was considered statistically significant.

Results

Cell Uptake and Competitive Inhibition Experiments

Cellular uptake experiments showed that R-[18F]FPA and S-[18F]FPA uptake gradually increased in the HepG2 cells from 5 to 90 min (Fig. 1a). There were no significant differences between the uptake of R-[18F]FPA and S-[18F]FPA in HepG2 cells over 90 min ($P > 0.05$). To confirm the hypothesis that RS-[18F]FPA, S-[18F]FPA, and R-[18F]FPA uptake is related to FASN expression in tumors, an *in vitro* blocking study with orlistat was performed with HepG2 cells. Compared with uptake in the control group, the accumulation of RS-[18F]FPA, S-[18F]FPA, and R-[18F]FPA was inhibited by 46.5 %, 39.0 %, and 43.2 %, respectively, after the addition of 400 μM orlistat ($P < 0.05$) (Fig. 1b). To evaluate the contribution of the TCA cycle to the cellular uptake of RS-[18F]FPA, S-[18F]FPA, and R-[18F]FPA, 3-NP was used to treat HepG2 cells. Radioactivity uptake was inhibited by 35.3 %, 37.4 %, and 36.3 %, respectively, after the addition of 400 μM 3-NP ($P < 0.05$) (Fig. 1b). Further *in vitro* blocking studies with various concentrations of orlistat and 3-NP were performed on HepG2 cells to assess RS-[18F]FPA uptake. At 30 min, treatment with 25, 50, 100, 200, and 400 μM orlistat inhibited RS-[18F]FPA uptake into cells by 18.5 %, 26.1 %, 31.5 %, 36.5 %, and 46.5 % ($P < 0.05$), respectively (as shown in Fig. 1c). At 30 min, the 3-NP-treated cells (at the same concentrations as above) showed RS-[18F]FPA uptake inhibition of 18.4 %, 19.4 %, 35.9 %, 35 %, and 35.3 % ($P < 0.05$), respectively (Fig. 1d). Similar cell uptake and competitive inhibition experimental results were observed in SK-Hep-1 cell lines (Suppl. Fig. 1, see Electronic Supplementary Material (ESM)).

Small-Animal PET Study

Small-animal PET imaging with RS-[18F]FPA, S-[18F]FPA, R-[18F]FPA, and [18F]FDG was performed on HepG2 tumor-bearing mice ($n = 5$) (Fig. 2a). The average tumor uptake values for RS-[18F]FPA, S-[18F]FPA, R-[18F]FPA, and [18F]FDG at 90 min postinjection were 6.63 ± 0.10, 5.60 ± 0.13, 6.68 ± 0.25, and 3.65 ± 0.65 % ID/g, respectively, the average uptake values of these tracers in muscle were 2.82 ± 0.80, 2.60 ± 0.50, 2.79 ± 0.17, and 1.83 ± 0.38 % ID/g, respectively, and the average uptake values in liver were 4.88 ± 0.97, 4.91 ± 0.65, 4.78 ± 0.23, and 3.17 ± 0.12 % ID/g, respectively. The uptake of R-[18F]FPA and RS-[18F]FPA in tumors was not significantly different ($P > 0.05$), but there was a marked difference between that of R-[18F]FPA and S-[18F]FPA in tumor uptake ($P < 0.05$). RS-[18F]FPA, S-[18F]FPA, and R-[18F]FPA had higher tumor-to-muscle (T/M) and tumor-to-liver (T/L) uptake ratios than 18F-FDG at 90 min postinjection, and the T/M and T/L uptake ratios of R-[18F]FPA were significantly higher than those of S-[18F]FPA ($P < 0.05$) (Fig. 2b).

PET images of R-[18F]FPA obtained in HepG2 tumor-bearing mice ($n = 3$) at different time points are shown in Fig. 3. The PET studies show that the uptake of R-[18F]FPA reached a peak at 90 min postinjection, and the radioactivity uptake values in the tumors were 6.07 ± 0.05, 7.07 ± 0.05, 7.13 ± 0.05, and 7.08 ± 0.04 % ID/g at 30, 60, 90, and 120 min postinjection, respectively (Fig. 3a, b). In addition to the tumors, the liver showed high uptake values from 30 to 120 min postinjection, but the uptake by the liver was not significantly different between the four different time points ($P > 0.05$) (Fig. 3b). Muscle radioactivity was relatively low and evenly distributed during the 120 min after injection (Fig. 3b). The uptake of R-[18F]FPA in HepG2 tumors was significantly higher than that of [18F]FDG at 60 min postinjection (7.07 ± 0.05 *vs.* 4.30 ± 0.19, $P < 0.05$) (Fig. 3c).

PET imaging of tumors of different sizes using R-[18F]FPA and [18F]FDG was performed on HepG2 and SK-Hep-1 tumor-bearing mice. The PET studies showed that the uptake of R-[18F]FPA was lower than that of [18F]FDG in large HepG2 tumors (diameter of approximately 10 mm) at 90 min after injection (8.30 ± 0.08 % ID/g *vs.* 9.30 ± 0.15 % ID/g, $P < 0.05$) (Fig. 4a). Meanwhile, the T/M uptake ratio of [18F]FDG in the large HepG2 tumors was significantly higher than that of R-[18F]FPA at 90 min postinjection (6.54 ± 0.52 *vs.* 2.77 ± 0.22, $P < 0.05$), and the T/L uptake ratio of [18F]FDG was significantly higher than that of R-[18F]FPA (3.10 ± 0.13 *vs.* 1.60 ± 0.13, $P < 0.05$), as shown in Fig. 4b. However, the uptake values for R-[18F]FPA in small HepG2 tumors (diameter of approximately 5 mm) were higher than those of [18F]FDG at 90 min after injection (7.00 ± 0.23 % ID/g *vs.* 3.20 ± 0.11 % ID/g, $P < 0.05$) (Fig. 4d). Moreover, the T/M uptake ratio of R-[18F]FPA in small HepG2 tumors was higher than that of [18F]FDG at 90 min postinjection (2.30 ± 0.21 *vs.* 2.00 ± 0.12, $P < 0.05$), and the T/L uptake ratio of R-[18F]FPA was higher than that of [18F]FDG (1.89 ± 0.13 *vs.* 1.60 ± 0.20, $P < 0.05$), as shown in Fig. 4e. The uptake of R-[18F]FPA was higher than that of [18F]FDG in both relative small SK-Hep-1 tumors (6.85 ± 0.21 % ID/g *vs.* 2.89 ± 0.18 % ID/g, $P < 0.05$; Fig. 5a) and large SK-Hep-1 tumors (8.85 ± 0.39 % ID/g *vs.* 6.23 ± 0.28 % ID/g, $P < 0.05$; Fig. 5b) at 60 min after injection. The T/M uptake ratios of R-[18F]FPA was higher than that of [18F]FDG in both small SK-Hep-1 tumors (2.45 ± 0.19 *vs.* 1.93 ± 0.13, $P < 0.05$) and large SK-Hep-1 tumors (3.88 ± 0.20 *vs.* 3.46 ± 0.40, $P < 0.05$) at 60 min post-

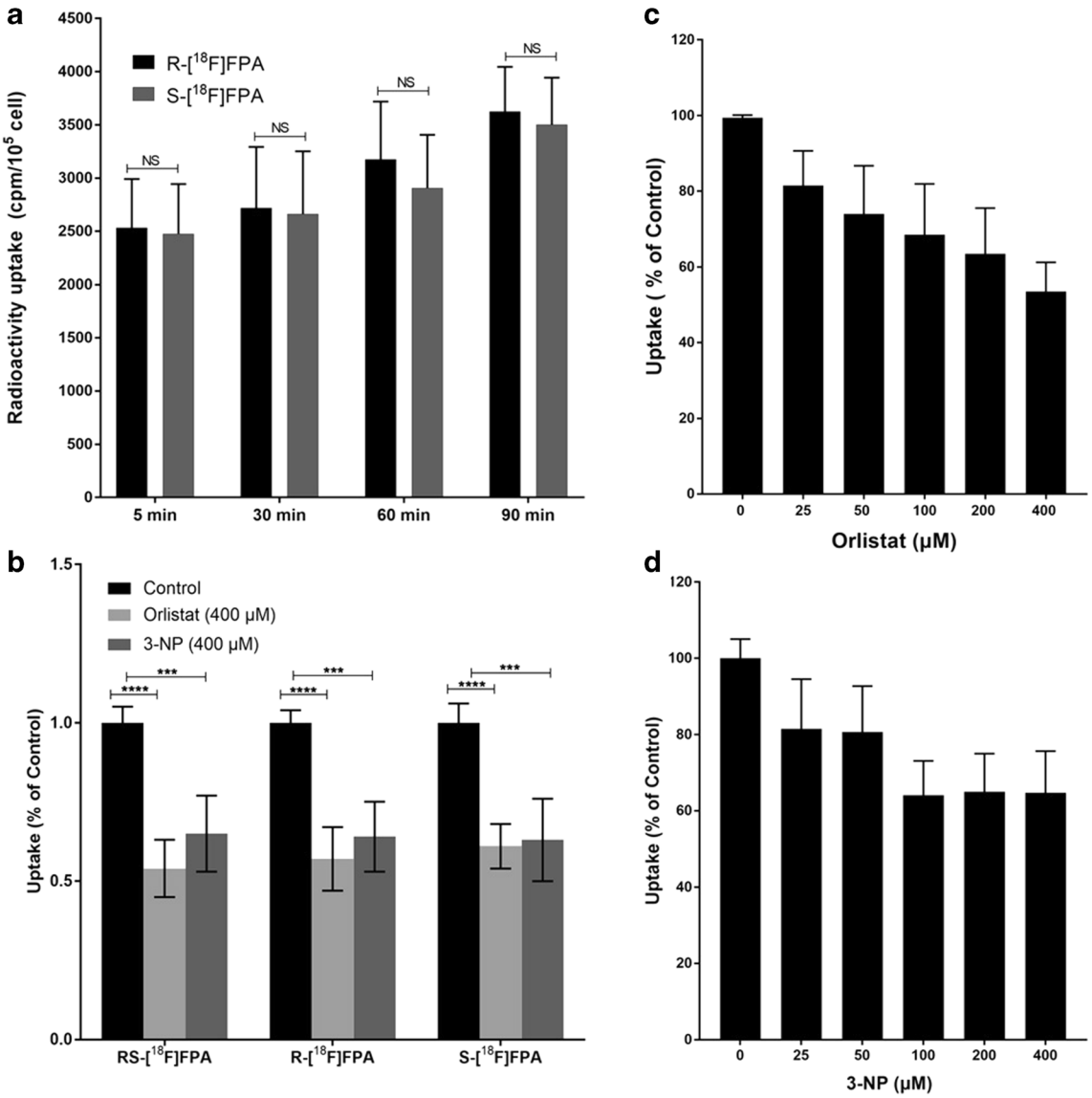

Fig. 1 **a** R-[18F]FPA and S-[18F]FPA uptake in HepG2 cells at different time points. **b** The results for RS-[18F]FPA, S-[18F]FPA, and R-[18F]FPA uptake by HepG2 cells inhibited by 400 μM orlistat and 400 μM 3-NP. **c** The results for RS-[18F]FPA uptake by HepG2 cells inhibited with different concentrations of orlistat. **d** The results for RS-[18F]FPA uptake by HepG2 cells inhibited with different concentrations of 3-NP.

injection, and the T/L uptake ratios of R-[18F]FPA was also higher than that of [18F]FDG (1.81 ± 0.12 *vs.* 1.45 ± 0.21, 2.39 ± 0.14 *vs.* 2.07 ± 0.18, $P < 0.05$), as shown in Fig. 5c, d.

Biodistribution of R-[18F]FPA in HepG2 Tumor-Bearing Mice

The biodistribution of R-[18F]FPA in HepG2 tumor-bearing mice was investigated at 30, 60, 90, and 120 min after injection (Suppl. Fig. 2 in ESM). The results showed that the uptake of R-[18F]FPA in tumors gradually increased over 60 min, and then relatively stable levels of radioactivity uptake were maintained from 60 to 120 min. The radioactivity uptake rates of R-[18F]FPA in the tumors were 3.80 ± 0.55, 4.52 ± 0.35, 4.14 ± 0.65, and 4.28 ± 0.61 % ID/g at 30, 60, 90, and 120 min postinjection, respectively. The elimination of tracer from the blood was relatively slow, changing from 2.84 ± 0.12 % ID/g at 30 min to 2.49 ± 0.10 % ID/g at 120 min after injection. A moderate uptake rate and slow clearance of radioactivity were found in the organs and tissues of interest (brain, lungs, heart, liver, stomach, spleen, muscle, and bone) from 30 to 120 min. Supplementary Fig. 2b in ESM shows the tumor-to-organ ratio of R-[18F]FPA at 30, 60, 90, and 120 min after injection. The tumor-to-organ ratio is greater than 1 for all of the organs.

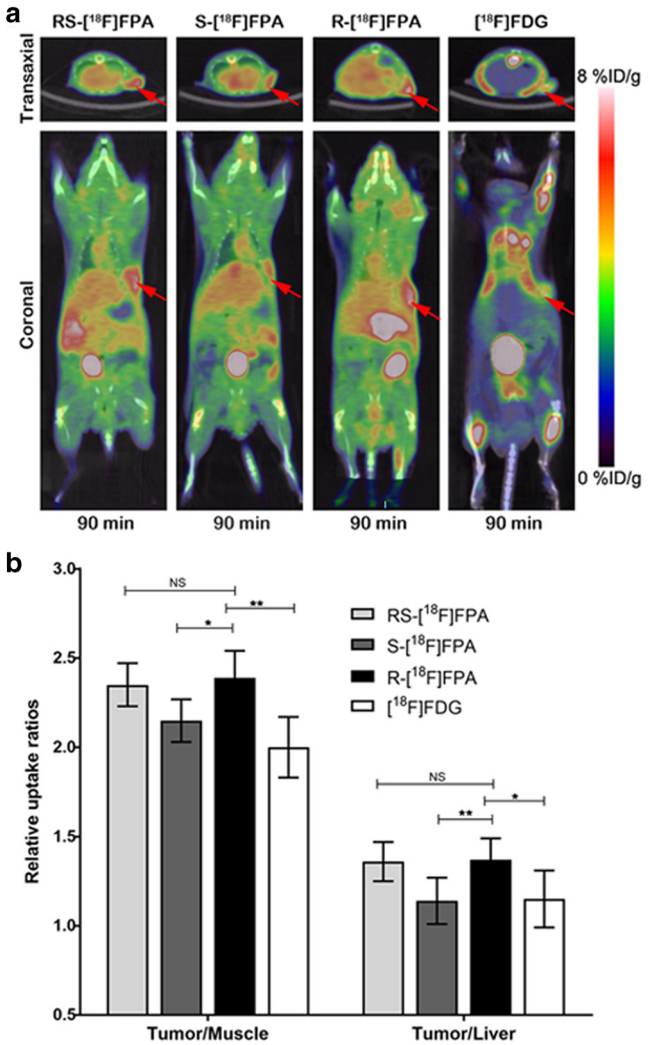

Fig. 2 **a** PET/CT fusion images of HepG2 tumor-bearing mice scanned 90 min postinjection with RS-[^{18}F]FPA, S-[^{18}F]FPA, R-[^{18}F]FPA, and [^{18}F]FDG ($n = 5$ mice per group, the red arrows point to the tumors). **b** The relative tumor-to-muscle (T/M) and tumor-to-liver (T/L) uptake ratios for RS-[^{18}F]FPA, S-[^{18}F]FPA, R-[^{18}F]FPA, and [^{18}F]FDG ($n = 5$ per group).

PET Imaging of Tumor-Bearing Mice with FASN and TCA Inhibition

HepG2 and SK-Hep-1 tumor-bearing mice were imaged with R-[^{18}F]FPA before and after treatment with orlistat or 3-NP. The uptake (% ID/g) of R-[^{18}F]FPA into HepG2 tumors decreased by 19.3 % after treatment with orlistat (8.30 ± 0.18 *vs.* 6.70 ± 0.12, $P < 0.05$) (Fig. 6a, b) and by 31.8 % after treatment with 3-NP (8.50 ± 0.21 *vs.* 5.80 ± 0.12, $P < 0.05$) (Fig. 6c, d). In normal tissues including the liver, brain, and muscle, the radioactivity uptake showed no marked reduction after treatment with orlistat or 3-NP ($P > 0.05$). The uptake of R-[^{18}F]FPA in SK-Hep-1 tumors was inhibited by 39.5 % with orlistat (8.85 ± 0.39 *vs.* 5.35 ± 0.26, $P < 0.05$; Fig. 5b, e).

Discussion

The increased glucose metabolism in tumors is mainly correlated with overexpression of glucose transporter-1 (GLUT1) [33–35]. However, the sensitivity of [^{18}F]FDG to detect well-differentiated liver cancer is low and may be correlated with the low expression of Glut-1 [33–35]. Cytoplasmic GLUT1 is overexpressed in the HepG2 cell line [36]. FASN is also overexpressed in the HepG2 cell line [37]. Therefore, we chose HepG2 cells to compare the PET imaging efficacy of [^{18}F]FDG, RS-[^{18}F]FPA, S-[^{18}F]FPA, and R-[^{18}F]FPA.

PET imaging studies demonstrated that HepG2 tumors can be successfully detected by RS-[^{18}F]FPA, S-[^{18}F]FPA, and R-[^{18}F]FPA, and the accumulation of all these tracers in HepG2 tumors was higher than that of [^{18}F]FDG. These experimental results showed that [^{18}F]FPA uptake in HepG2 tumors may be related to FASN expression. Among the tracers, there were no significant differences between the uptake of RS-[^{18}F]FPA and R-[^{18}F]FPA into the tumors, but the uptake of R-[^{18}F]FPA by tumors was clearly higher than that of S-[^{18}F]FPA, which is in agreement with our previous research [29]. Additionally, R-[^{18}F]FPA had better T/L and T/M uptake ratios than S-[^{18}F]FPA and [^{18}F]FDG. All these results show that R-[^{18}F]FPA is a useful tracer for PET imaging of tumors.

The PET studies also showed that R-[^{18}F]FPA rapidly accumulated in HepG2 tumors and that the uptake rate remained high from 60 to 120 min. The results suggested that the optimal time point for PET scanning was at least 60 min postinjection. The biodistribution results of R-[^{18}F]FPA in tumor-bearing mice showed that the accumulation of radioactivity gradually increased until peaking at 60 min, and then slightly decreased from 60 to 120 min postinjection. The biodistribution data for R-[^{18}F]FPA at different time points were not in complete agreement with the PET imaging results, which showed a relatively stable uptake rate of R-[^{18}F]FPA from 60 to 120 min. The reason for this phenomenon may be primarily attributed to the fact that animals were anesthetized during the PET scans, while the mice in the biodistribution study were active and without any anesthetic treatment until sacrifice. In addition, the PET imaging experiment used individuals from the same nude mouse model, while various mice with different sizes of the tumor were used in the biodistribution study. The uptake of R-[^{18}F]FPA in other normal organs was similar to that observed in previous research [29, 38]. The research results showed that R-[^{18}F]FPA had a relatively wide imaging time window and high tumor-to-non-target ratios. Especially, as an optically pure compound, R-[^{18}F]FPA seemed to show greater potential as a fatty acid PET tracer for detecting liver cancer than RS-[^{18}F]FPA in clinical settings.

Previous studies have reported that propionate is an energy-providing substrate for heart and tumor cells and that the metabolic mechanism for propionate metabolism may begin with the synthesis of fatty acids [26, 27]. Several

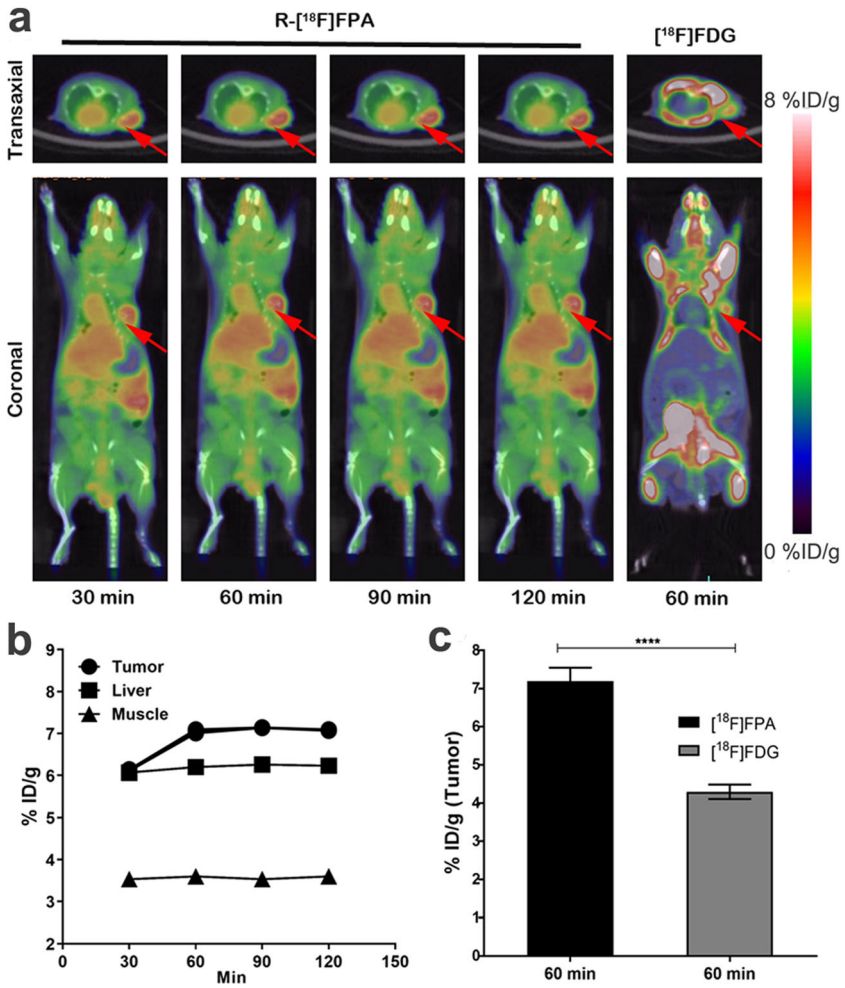

Fig. 3 **a** R-[^{18}F]FPA PET/CT fusion images of HepG2 tumor-bearing mice scanned at 30, 60, 90, and 120 min postinjection and [^{18}F]FDG PET/CT fusion images of the same mice at 60 min postinjection ($n = 3$ mice per group, the red arrows show the tumors). **b** The corresponding R-[^{18}F]FPA uptake (% ID/g) of tumors and the organs of interest at 30, 60, 90, and 120 min postinjection. **c** The corresponding uptake (% ID/g) of R-[^{18}F]FPA and [^{18}F]FDG in the tumors 60 min postinjection.

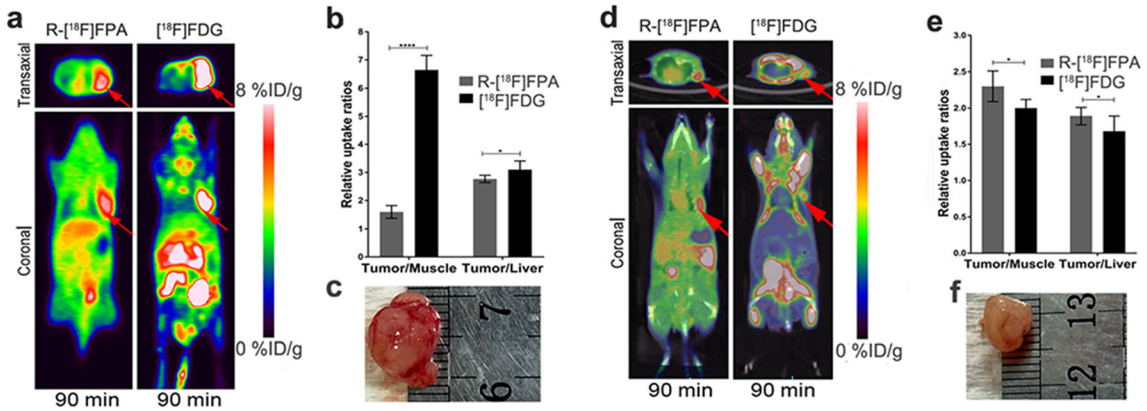

Fig. 4 **a** R-[^{18}F]FPA and [^{18}F]FDG PET/CT fusion images of HepG2 tumor-bearing mice with tumors approximately 10 mm diameter at 90 min postinjection ($n = 3$ mice per group, the red arrows show the tumors). **b** The tumor-to-muscle (T/M) and tumor-to-liver (T/L) uptake ratios of R-[^{18}F]FPA and [^{18}F]FDG in tumors approximately 10 mm in diameter. **c** Photo of tumor tissue. **d** R-[^{18}F]FPA and [^{18}F]FDG PET/CT fusion images of HepG2 tumor-bearing mice with tumors approximately 5 mm in diameter ($n = 3$ mice per group, the red arrows point to the tumors). **e** The relative T/M and T/L uptake ratios of R-[^{18}F]FPA and [^{18}F]FDG in tumors approximately 5 mm in diameter. **f** Photo of tumor tissue.

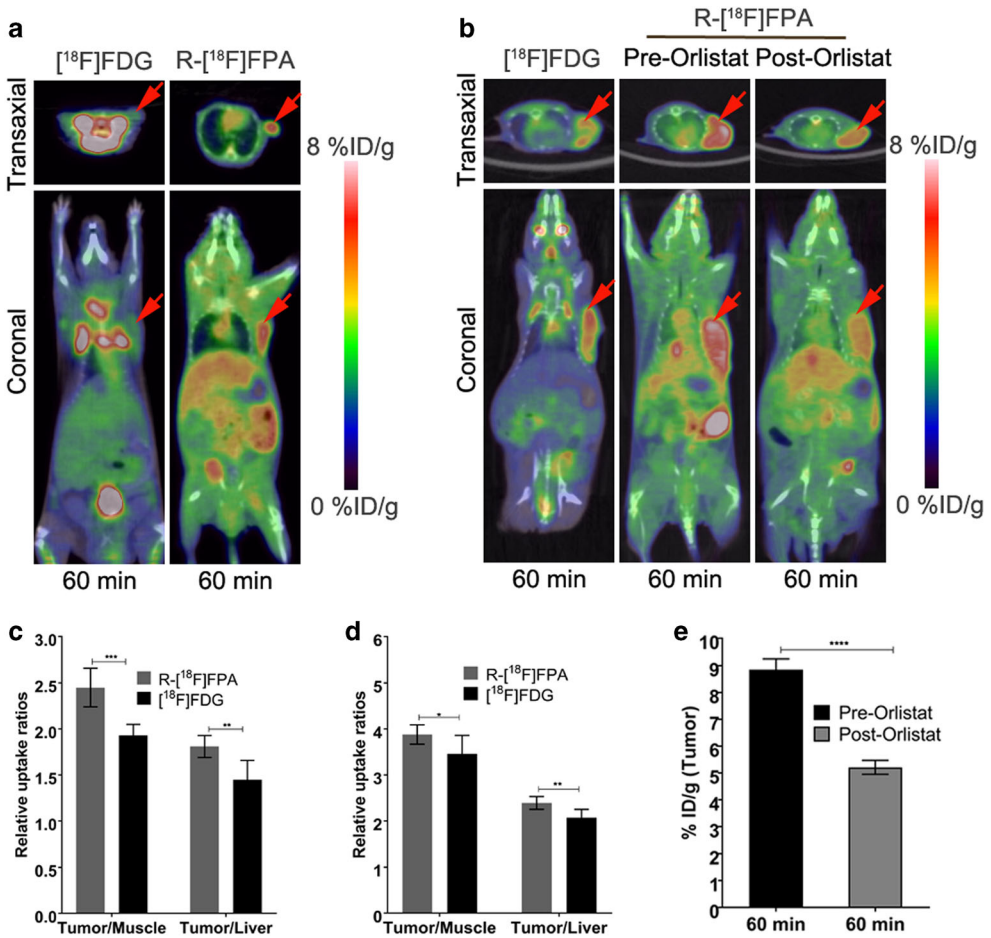

Fig. 5 **a** R-[18F]FPA and [18F]FDG PET/CT fusion images of SK-Hep-1 tumor-bearing mice with small tumors at 60 min postinjection ($n = 3$ mice per group, the red arrows show the tumors). **b** R-[18F]FPA and [18F]FDG PET/CT fusion images of SK-Hep-1 tumor-bearing mice with large tumors at 60 min postinjection ($n = 3$ mice per group, the red arrows show the tumors). R-[18F]FPA PET images of SK-Hep-1 tumor-bearing mice with and without orlistat treatment at 60 min postinjection ($n = 3$ mice per group). **c** The corresponding uptake (% ID/g) of R-[18F]FPA and [18F]FDG in the small tumors 60 min postinjection. **d** The corresponding uptake (% ID/g) of R-[18F]FPA and [18F]FDG in the large tumors 60 min postinjection. **e** The corresponding radioactivity uptake (% ID/g) of R-[18F]FPA in tumor, 60 min postinjection after treatment with or without orlistat.

studies have shown that [18F]FPA and [18F]FAC may be metabolized *via* similar mechanisms [16, 38]. Unlike the significant defluorination of [18F]FAC, RS-[18F]FPA and its two enantiomers demonstrated no evidence of defluorination throughout the whole experiment, suggesting that [18F]FAC and [18F]FPA are involved in different metabolic pathways.

Inhibition of FASN by orlistat or of succinate dehydrogenase (SDH) by 3-NP can decrease fatty acid synthesis or the rate of the TCA cycle, respectively [9, 39]. Under the same concentrations of orlistat and 3-NP, the degrees of inhibition of RS-[18F]FPA, R-[18F]FPA and S-[18F]FPA uptake in HepG2 and SK-Hep-1 cells were similar, suggesting that RS-[18F]FPA and its two enantiomers are taken up *via* similar mechanisms in the HepG2 and SK-Hep-1 cell lines. The orlistat-treated cells showed clearly decreased rates of RS-[18F]FPA uptake under different concentrations of the inhibitor when compared with the control groups, which indicated that RS-[18F]FPA may be involved in fatty acid synthesis [9]. In our study, a marked reduction in RS-[18F]FPA uptake was found after the treatment of HepG2 and SK-Hep-1 cells with different concentrations of the inhibitor 3-NP, which indicated that RS-[18F]FPA may be involved in the TCA cycle. PET analysis of competitive inhibition also demonstrated that the *in vivo* uptake of R-[18F]FPA into HepG2 tumor-bearing mice was strongly inhibited by orlistat and 3-NP, which further confirmed that the mechanism of R-[18F]FPA uptake may also be involved in fatty acid synthesis and the TCA cycle. However, the *in vitro* cellular uptake experiment found that HepG2 and SK-Hep-1 cells continued to take up R-[18F]FPA, even under high concentrations of the inhibitors. Meanwhile, the *in vivo* PET imaging showed similar results; R-[18F]FPA uptake in the tumors decreased after treatment with orlistat or 3-NP, but high rates of radioactivity uptake were still present in tumors under high concentrations of the inhibitors. Therefore, it is possible that R-

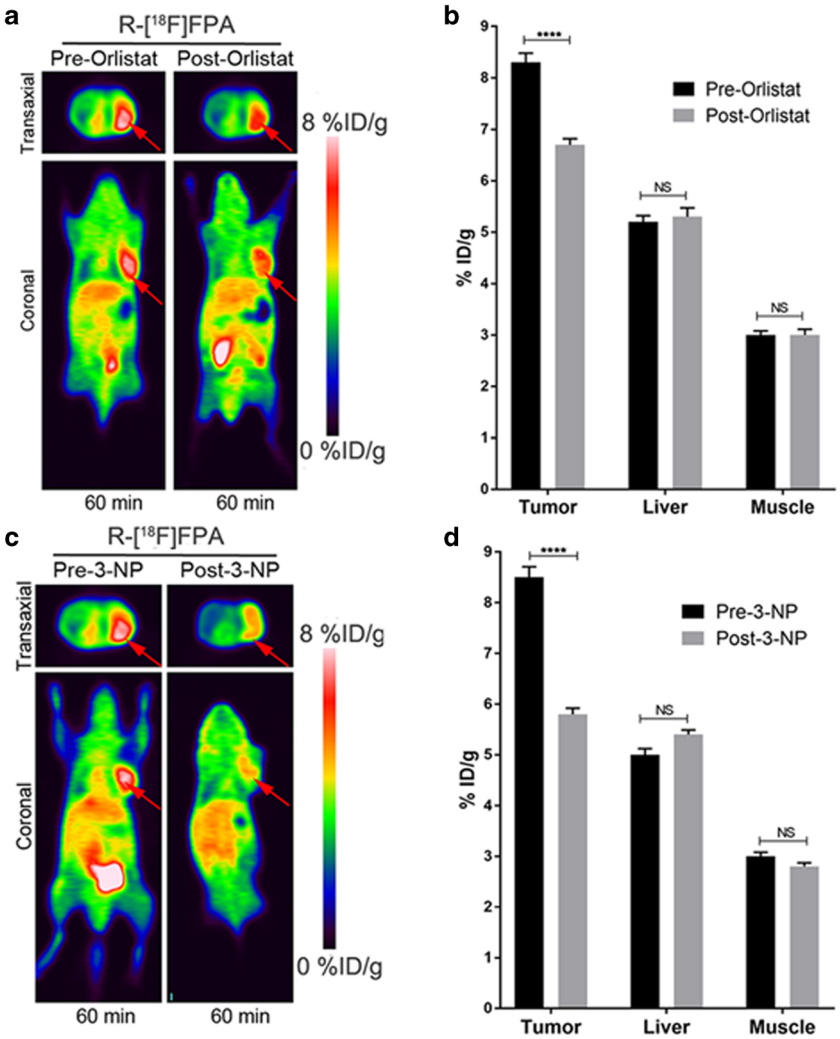

Fig. 6 **a** R-[18F]FPA PET images of HepG2 tumor-bearing mice with and without of orlistat treatment at 60 min postinjection ($n = 3$ mice per group). **b** The corresponding radioactivity uptake (% ID/g) of R-[18F]FPA into tumor, liver, and muscle tissue 60 min postinjection after treatment with orlistat. **c** R-[18F]FPA PET images of HepG2 tumor-bearing mice with and without 3-NP treatment at 60 min postinjection ($n = 3$ mice per group). **d** The corresponding radioactivity uptake (% ID/g) of R-[18F]FPA in tumor, liver, and muscle tissues 60 min postinjection after treatment with or without 3-NP.

[18F]FPA uptake into tumors also involves other mechanisms. Additionally, R-[18F]FPA and S-[18F]FPA had similar uptake rates in HepG2 and SK-Hep-1 cells for the *in vitro* cell uptake experiments, while the uptake rates of R-[18F]FPA and S-[18F]FPA appeared significantly different for *in vivo* PET imaging. The different *in vivo* radioactivity uptake rates between R-[18F]FPA and S-[18F]FPA may be due to the presence of different mechanism in the more complicated *in vivo* microenvironment in addition to their similar uptake mechanisms related to FASN and the TCA cycle [40]. Alternatively, perhaps there existed with difference in metabolism of the radiotracer (*e.g.*, plasma clearance) and with difference in uptake and/or incorporation in fatty acid synthesis, of course, which need to be further studied in our next work. *In vivo* FASN inhibition studies demonstrated that R-[18F]FPA involved in the same metabolic pathway in both SK-Hep-1 and HepG2 tumors but exhibited a higher sensitivity to inhibition by orlistat in SK-Hep-1 tumors with higher levels of FASN [41].

A previous study reported that [18F]FDG and [11C]acetate PET have low sensitivities in detecting small liver cancer [23]. Our micro-PET studies showed that both R-[18F]FPA and [18F]FDG resulted in high levels of radioactivity accumulation in the detection of large tumors (10 mm in diameter). However, the sensitivity of R-[18F]FPA was clearly higher than that of [18F]FDG in the detection of tumor lesions with a size smaller or equal to 5 mm in diameter, indicating that R-[18F]FPA PET was significantly superior to [18F]FDG PET in detecting small tumors (both SK-Hep-1 and HepG2 tumors). Moreover, research has shown that increased expression of FASN was found in early steps of mammary carcinogenesis [42]. Therefore, R-

[18F]FPA may be a better potential PET probe for detecting liver cancer at an early stage, which could be due to the dominance of fatty acid synthesis over glucose metabolism in early tumor cell proliferation [8], with low GLUT1 expression and an overexpression of FASN in the early stages of liver cancer [6, 41, 42].

Conclusion

The potential PET imaging value of R-[18F]FPA in detecting liver cancer is similar to that of RS-[18F]FPA but superior to that of S-[18F]FPA. Micro-PET imaging results show that R-[18F]FPA is more sensitive than [18F]FDG in detecting small liver cancer in tumor-bearing nude mice and can effectively compensate for the deficiencies of [18F]FDG. Overall, R-[18F]FPA, as an optically pure tracer, seems to be a more suitable metabolic PET tracer than S-[18F]FPA for detecting liver cancer, particularly in the early stages of tumors. In addition, the metabolic pathways for [18F]FPA may involve the TCA cycle and fatty acid synthesis in liver cancer. But the details of these mechanisms still need to be further investigated.

Funding information. This study was funded by the National Natural Science Foundation of China (No. 81571704, No. 81371584), the Science and Technology Foundation of Guangdong Province (No. 2016B090920087, No. 2014A020210008), the Science and Technology Planning Project Foundation of Guangzhou (No. 201604020169), and the China Postdoctoral Science Foundation (CPSF) (No.2018M631029 to S Liu).

Compliance with Ethical Standards

The experiments were approved by the Institutional Animal Care and Utilization Committee (IACUU) of the First Affiliated Hospital, Sun Yat-sen University (approval no. 2016058).

Conflict of Interest

The authors declare that they have no conflict of interest.

References

1. Rahib L, Smith BD, Aizenberg R, Rosenzweig AB, Fleshman JM, Matrisian LM (2014) Projecting cancer incidence and deaths to 2030: the unexpected burden of thyroid, liver, and pancreas cancers in the United States. Cancer Res 74:2913–2921
2. Benson AB 3rd, D'Angelica MI, Abrams TA et al (2014) Hepatobiliary cancers, version 2. 2014. J Natl Compr Cancer Netw 12:1152–1182
3. Kremer N, Walther AE, Tiao GM (2014) Management of hepatoblastoma: an update. Curr Opin Pediatr 26:362–369
4. Bolog N, Andreisek G, Oancea I, Mangrau A (2011) CT and MR imaging of hepatocellular carcinoma. J Gastrointestin Liver Dis 20:181–189
5. Chotipanich C, Kunawudhi A, Promteangtrong C, Tungsuppawattanakit P, Sricharunrat T, Wongsa P (2016) Diagnosis of hepatocellular carcinoma using C-11 choline PET/CT: comparison with F-18FDG, contrast-enhanced MRI and MDCT. Asian Pac J Cancer Prev 17:3569–3573
6. Trojan J, Schroeder O, Raedle J, Baum RP, Herrmann G, Jacobi V, Zeuzem S (1999) Fluorine-18 FDG positron emission tomography for imaging of hepatocellular carcinoma. Am J Gastroenterol 94:3314–3319
7. Wu HB, Wang QS, Li BY, Li HS, Zhou WL, Wang QY (2011) F-18 FDG in conjunction with 11C-choline PET/CT in the diagnosis of hepatocellular carcinoma. Clin Nucl Med 36:1092–1097
8. Plathow C, Weber WA (2008) Tumor cell metabolism imaging. J Nucl Med 49(Suppl 2):43S–63S
9. Yoshii Y, Furukawa T, Oyama N, Hasegawa Y, Kiyono Y, Nishii R, Waki A, Tsuji AB, Sogawa C, Wakizaka H, Fukumura T, Yoshii H, Fujibayashi Y, Lewis JS, Saga T (2013) Fatty acid synthase is a key target in multiple essential tumor functions of prostate cancer: uptake of radiolabeled acetate as a predictor of the targeted therapy outcome. PLoS One 8:e64570
10. Deford-Watts LM, Mintz A, Kridel SJ (2013) The potential of 11C-acetate PET for monitoring the fatty acid synthesis pathway in tumors. Curr Pharm Biotechnol 14:300–312
11. Yoshii Y, Furukawa T, Saga T, Fujibayashi Y (2015) Acetate/acetyl-CoA metabolism associated with cancer fatty acid synthesis: overview and application. Cancer Lett 356:211–216
12. Ho CL, Yu SC, Yeung DW et al (2003) 11C-acetate PET imaging in hepatocellular carcinoma and other liver masses. J Nucl Med 44:213–221
13. Hwang KH, Choi DJ, Lee SY, Lee MK, Choe W (2009) Evaluation of patients with hepatocellular carcinomas using [11C]acetate and [18F]FDG PET/CT: a preliminary study. Appl Radiat Isot 67:1195–1198
14. Salem N, Kuang Y, Wang F, Maclennan GT, Lee Z (2009) [(Methyl)1-11C]-acetate metabolism in hepatocellular carcinoma. Q J Nucl Med Mol Imaging 53:144–156
15. Bertagna F, Bertoli M, Bosio G, Biasiotto G, Sadeghi R, Giubbini R, Treglia G (2014) Diagnostic role of radiolabelled choline PET or PET/CT in hepatocellular carcinoma: a systematic review and meta-analysis. Hepatol Int 8:493–500
16. Takemoto K, Hatano E, Nishii R, Kagawa S, Kishibe Y, Takahashi M, Yamauchi H, Matsumura K, Zaima M, Toriguchi K, Tanabe K, Kitamura K, Seo S, Taura K, Endo K, Uemoto S, Higashi T (2014) Assessment of [18F]-fluoroacetate PET/CT as a tumor-imaging modality: preclinical study in healthy volunteers and clinical evaluation in patients with liver tumor. Ann Nucl Med 28:371–380
17. Yamamoto Y, Nishiyama Y, Kameyama R, Okano K, Kashiwagi H, Deguchi A, Kaji M, Ohkawa M (2008) Detection of hepatocellular carcinoma using 11C- choline PET: comparison with 18F-FDG PET. J Nucl Med 49:1245–1248
18. Talbot JN, Gutman F, Fartoux L, Grange JD, Ganne N, Kerrou K, Grahek D, Montravers F, Poupon R, Rosmorduc O (2006) PET/CT in patients with hepatocellular carcinoma using [18F] fluorocholine: preliminary comparison with [18F]FDG PET/CT. Eur J Nucl Med Mol Imaging 33:1285–1289
19. Ho CL, Cheung MK, Chen S, Cheung TT, Leung YL, Cheng KC, Yeung WD (2012) [18F]fluoroacetate positron emission tomography for hepatocellular carcinoma and metastases: an alternative tracer for [11C]acetate? Mol Imaging 11:229–239
20. Kuang Y, Salem N, Tian H, Kolthammer JA, Corn DJ, Wu C, Wang F, Wang Y, Lee Z (2011) Imaging lipid synthesis in hepatocellular carcinoma with [methyl-11C]choline: correlation with in vivo metabolic studies. J Nucl Med 52:98–106
21. Kwee SA, Sato MM, Kuang Y, Franke A, Custer L, Miyazaki K, Wong LL (2017) [18F]fluorocholine PET/CT imaging of liver cancer: radiopathologic correlation with tissue phospholipid profiling. Mol Imaging Biol 19:446–455
22. Li L, Che L, Wang CM, Blecha JE, Li X, VanBrocklin HF, Calvisi DF, Puchowicz M, Chen X, Seo Y (2016) [11C]acetate PET imaging is not always associated with increased lipogenesis in hepatocellular carcinoma in mice. Mol Imaging Biol 18:360–367
23. Park JW, Kim JH, Kim SK, Kang KW, Park KW, Choi JI, Lee WJ, Kim CM, Nam BH (2008) A prospective evaluation of 18F-FDG and 11C-acetate PET/CT for detection of primary and metastatic hepatocellular carcinoma. J Nucl Med 49:1912–1921
24. Vāvere AL, Kridel SJ, Wheeler FB et al (2008) 1-11C-acetate as a PET radiopharmaceutical for imaging fatty acid synthase expression in prostate Cancer. J Nucl Med 49:327–334
25. Pillarsetty N, Punzalan B, Larson SM (2009) 2-18F-Fluoropropionic acid as a PET imaging agent for prostate cancer. J Nucl Med 50:1709–1714

26. Kasumov T, Cendrowski AV, David F, Jobbins KA, Anderson VE, Brunengraber H (2007) Mass isotopomer study of anaplerosis from propionate in the perfused rat heart. Arch Biochem Biophys 463:110–117
27. Kridel SJ, Lowther WT, Pemble CW (2007) Fatty acid synthase inhibitors: new directions for oncology. Expert Opin Investig Drugs 16:1817–1829
28. Bastiaansen JA, Cheng T, Mishkovsky M et al (2013) In vivo enzymatic activity of acetylCoA synthetase in skeletal muscle revealed by ^{13}C turnover from hyperpolarized [1-^{13}C]acetate to [1-^{13}C]acetylcarnitine. Biochim Biophys Acta 1830:4171–4178
29. Zhang ZW, Liu SY, Tang XL, Nie D, Tang G, Sun A, Xiong Y, Ma H, Wen F, Hu P (2018) Radiosynthesis and preliminary biological evaluation of the 2-[^{18}F]fluoropropionic acid enantiomers for tumor PET imaging. J Radi Nucl Chem 316:153–159
30. Zhao J, Zhang ZW, Nie DH et al (2019) PET imaging of hepatocellular carcinomas:^{18}F-fluoropropionic acid as a complementary radiotracer for ^{18}F-fluorodeoxyglucose. Mol Imaging 18:1–8
31. Wang HL, Hu KZ, Tang GH et al (2012) Simple and efficient automated radiosynthesis of 2-^{18}F-fluoropropionic acid using solid-phase extraction cartridges purification. J Label Compd Radiopharm 55:366–370
32. Olsen C, Rustad A, Fonnum F, Paulsen RE, Hassel B (1999) 3-Nitropropionic acid: an astrocyte-sparing neurotoxin in vitro. Brain Res 850:144–149
33. Khan MA, Combs CS, Brunt EM, Lowe VJ, Wolverson MK, Solomon H, Collins BT, Bisceglie AMD (2000) Positron emission tomography scanning in the evaluation of hepatocellular carcinoma. J Hepatol 32:792–797
34. Yen TC, See LC, Lai CH, Yah-Huei CW, Ng KK, Ma SY, Lin WJ, Chen JT, Chen WJ, Lai CR, Hsueh S (2004) ^{18}F-FDG uptake in squamous cell carcinoma of the cervix is correlated with glucose transporter 1 expression. J Nucl Med 45:22–29
35. Lee JD, Yang WI, Park YN, Kim KS, Choi JS, Yun M, Ko D, Kim TS, Cho AE, Kim HM, Han KH, Im SS, Ahn YH, Choi CW, Park JH (2005) Different glucose uptake and glycolytic mechanisms between hepatocellular carcinoma and intrahepatic mass-forming cholangiocarcinoma with increased ^{18}F-FDG uptake. J Nucl Med 46:1753–1759
36. Brito AF, Abrantes AM, Ribeiro M, Oliveira R, Casalta-Lopes J, Gonçalves AC, Sarmento-Ribeiro AB, Tralhão JG, Botelho MF (2015) Fluorine-18 fluorodeoxyglucose uptake in hepatocellular carcinoma: correlation with glucose transporters and p53 expression. J Clin Exp Hepatol 5:183–189
37. Impheng H, Pongcharoen S, Richert L, Pekthong D, Srisawang P (2014) The selective target of capsaicin on FASN expression and de novo fatty acid synthesis mediated through ROS generation triggers apoptosis in HepG2 cells. PLoS One 9:e107842
38. Wang H, Tang G, Hu K, Huang T, Liang X, Wu Z, Li S (2016) Comparison of three ^{18}F-labeled carboxylic acids with ^{18}F-FDG of the differentiation tumor from inflammation in model mice. BMC Med Imaging 16:2
39. Henry PG, Lebon V, Vaufrey F, Brouillet E, Hantraye P, Bloch G (2002) Decreased TCA cycle rate in the rat brain after acute 3-NP treatment measured by in vivo 1H-{13C} NMR spectroscopy. J Neurochem 82:857–866
40. Impheng H, Richert L, Pekthong D, Scholfield CN, Pongcharoen S, Pungpetchara I, Srisawang P (2015) [6]-Gingerol inhibits de novo fatty acid synthesis and carnitine palmitoyltransferase-1 activity which triggers apoptosis in HepG2. Am J Cancer Res 5:1319–1336
41. Hao Q, Li T, Zhang X et al (2014) Expression and roles of fatty acid synthase in hepatocellular carcinoma. Oncol Rep 32:2471–2476
42. Esslimani-Sahla M, Thezenas S, Simony-Lafontaine J, Kramar A, Lavaill R, Chalbos D, Rochefort H (2007) Increased expression of fatty acid synthase and progesterone receptor in early steps of human mammary carcinogenesis. Int J Cancer 120:224–229